RSC Advances

This is an *Accepted Manuscript*, which has been through the Royal Society of Chemistry peer review process and has been accepted for publication.

Accepted Manuscripts are published online shortly after acceptance, before technical editing, formatting and proof reading. Using this free service, authors can make their results available to the community, in citable form, before we publish the edited article. This *Accepted Manuscript* will be replaced by the edited, formatted and paginated article as soon as this is available.

You can find more information about *Accepted Manuscripts* in the Information for Authors.

Please note that technical editing may introduce minor changes to the text and/or graphics, which may alter content. The journal's standard Terms & Conditions and the Ethical guidelines still apply. In no event shall the Royal Society of Chemistry be held responsible for any errors or omissions in this *Accepted Manuscript* or any consequences arising from the use of any information it contains.

ROYAL SOCIETY OF CHEMISTRY

www.rsc.org/advances

Zinc-Bromine Hybrid Flow Battery: Effect of Zinc Utilization and Performance Characteristics

S. Suresh, T. Kesavan, Y. Munaiah, I. Arul raj, S. Dheenadayalan*, P. Ragupathy*

Fuel Cells Section and Electrochemical Power Sources,
CSIR-Central Electrochemical Research Institute,
Karaikudi-630 006, India

* To whom all correspondence should be addressed,
E-mail: deenafc@gmail.com and ragupathyp@cecri.res.in
Tel: +91 04565 241361

RSC Advances Accepted Manuscript

Abstract

In order to achieve maximum efficiency and long life time of zinc bromine flow battery (ZBB), deposition and dissolution of zinc during the charging and discharging processes respectively is necessary to be in balance. In view of this, the percentage utilization of zinc during the discharge process is investigated in a zinc-bromine redox flow cell through potentio/galvanodynamic polarization test and electrochemical impedance spectroscopy. The cell employed carbon-plastic composite electrodes and 98 % pure zinc bromide electrolyte solution. The zinc bromine cells are charged at various current densities of 10, 20 and 30 $mAcm^{-2}$ and the deposited Zn during charging is compared with the dissolved zinc during the discharge process and found to be at 39, 41 and 39 % respectively. A 10 % increase in the zinc utilization factor is observed and this resulted in 17 % increase in the faradic efficiency when 99.9 % pure zinc bromide electrolyte solution is used. At the same time, 50 % utilization of zinc resulted in further 20 % increase in faradic efficiency in a cell with non porous graphite electrodes and 98 % pure zinc bromide salt solution. To qualify the nature of Zn deposit, XRD analysis is carried out along with other spectral studies. The basal plane of zinc (002) was observed at lower intensity peak whereas the plane (101) showed preferential growth in (101) direction. From these spectra, grain size and texture coefficient (TC) are also calculated in order to realize better Zn utilization in zinc bromine hybrid flow cell.

Keywords: zinc utilization; zinc bromine flow battery; efficiency; quaternary ammonium complexing agent

RSC Advances Accepted Manuscript

Introduction

Redox flow batteries are known to be the most compatible for grid energy storage system. In general, redox flow batteries theoretically have no performance loss because it relies on the electro-chemical reaction between electrolytes and not between the electrodes and electrolyte. Furthermore, one of the major advantages of this system is 100 % discharge capacity and can be left in this completely discharged state without damage, which means that the rated capacity is real capacity. Another advantage is decoupled energy and power as that of fuel cells.[1] The technical data of one among the promising system, zinc - bromine redox flow battery is 75-80% cycle efficiency, 80-85 $WhKg^{-1}$ energy density and with an unit design life time of 11-14 years[2]; this shows promise for use as an energy storage system for onsite power generation.

In spite of these favorable features of zinc - bromine redox flow battery, systematic studies of different aspects of its electrochemistry are scarce. Moreover, more studies were carried out on bromine electrochemistry and its utilization[3,4] than on zinc because of the fast reaction kinetics of zinc. Regardless of fast reaction kinetics of zinc when compared to bromine reaction, its reversibility is open to discussion, which is also considered to be one of the deciding factor for the overall cell performance characteristics. Hence, in the present study we have focused on the zinc electrochemical deposition/dissolution reaction in zinc bromine redox flow cell to realize improvement in the cell performance. First, we have conducted simple quantitative analyses of zinc deposition and dissolution in terms of capacity. Second, we explored the effect of substrate material and addition of complexing agents on zinc deposition/dissolution reaction with respect to improvement in the cell performance.

Experimental

RSC Advances Accepted Manuscript

The hardware used in this work was frameless carbon-plastic composite electrode with a geometric area of 50 cm^2 on both sides. 500 μm thick activated carbon active layer coating was applied on bromine electrode. Micro-porous polyethylene membrane (Daramic) with thickness 0.6 mm was used as separator. Temperature was maintained at 25 °C. The zinc electrolyte used in the work was 2 M zinc bromide (Alfa Aesar 98 % and 99.9 % purity) in 3 M NaCl (Alfa Aesar) as supporting electrolyte in order to eliminate ionic migration (i.e., no potential drop in the solution) and 0.8 M N-ethyl N-methyl pyrolidinium bromide as a complexing agent. Quantity of electrolyte used for circulation was 250 ml for each side. The electrolyte flow rate was 20 ml/min on both sides. Peristaltic pumps were used for electrolyte circulation. Test cell was assembled with the respective components as shown in Fig. 1.

Charging was carried out at a constant current density using Aplab testronic model 9313, India and discharge through load box model KM 0121, India. Time of charging was 15 min and cut off voltage during discharge at the same current density was 0.5 V. Characterization studies were carried out using a powder X-ray diffractometer in Philips XRD 'X' PERT PRO diffractometer with Cu Kα (α = 1.5418 Å) as a source at a scan rate of 0.5^o / min. The surface morphology of the deposits was examined by scanning electron microscopy (SEM, Vega-3 TESCA). Electrochemical impedance spectroscopy (10-2 Hz-105 Hz, amplitude = 5 mV) and cyclic voltammetry studies were carried out with VersaSTAT 3 instrument (Princeton Applied Research USA). The cycle life tests were performed in a cell controlled with BT-2000 work station (Arbin instruments USA). The XRD intensities of (hkl) planes were used to calculate the absolute texture coefficient (ATC) values through the following procedure.[5]

Intensities of the seven peaks were used to calculate intensity ratio

$$R_{(hk.l)} = [I_{(hk.l)}/\sum^{7}_{a=I} I_{(std)}]*100$$

RSC Advances Accepted Manuscript

By using these ratio values, texture coefficients for all seven planes were calculated through the equation $TC_{(hk.l)}=R_{(hk.l)}/R_{(std\ hk.l)}$ and ATC through the relation $ATC_{(hk.l)} = [TC_{(hk.l)}/\sum^{7}_{a=1} TC_{(hk.l)}]$ *100.

Results and Discussion

In order to calculate the amount of zinc deposited during the charging, and zinc dissolved during the discharging process, the test cell was dismantled and the cathode was removed as soon as after the charging process, for 15 min. After careful washing in triple distilled water and drying in vacuum oven at 60 °C for 10 min. the cathode containing zinc deposit was weighed. Thus, the calculated amounts of deposited zinc at current densities 10, 20 and 30 $mAcm^{-2}$ respectively were 0.136, 0.264 and 0.303 g. The amounts of zinc dissolved at the same load current densities till the cut off voltage of 0.5 V respectively were 0.054, 0.117 and 0.118 g, which, in terms of weight percentage amount to 39, 41 and 39 respectively. The interesting observation of these results is that almost 60 wt % of the deposited zinc remained unutilized irrespective of the load currents. This may be due to concomitant utilization of bromine at the anode or other reasons. Assuming that bromine is utilized concomitantly and considering the experimental results obtained at 10 $mAcm^{-2}$ current density; the amount of deposited zinc for 15 min time was 0.136 g. The theoretically calculated amount of zinc deposition for the same current density and time was 0.153 g. The difference being 0.017 g (11 %) of zinc, which is ascribed to the reason that the bromine crossover during charging process favoring the self discharge chemical reaction, namely, $Zn + Br_2 \leftrightarrow ZnBr_2$. There are two points which have to be considered before making conclusion 1) The flow pattern of the reactive species and 2) presence of complexing agent in both catholyte and anolyte. In the present study the adopted flow pattern was front flow hence bromine diffusion would not be much as with back flow pattern during

RSC Advances Accepted Manuscript

charging process[6] and the low amount of bromine crossed over will be complexed by the complexing agent in the catholyte. This was substantiated when the above result was compared with 0.009 g of zinc (6 %) that was obtained by using 99.9 % pure zinc bromide salt solution.

In a single charge - discharge cycle at a constant current density of 10 $mAcm^{-2}$, till the cut off voltage 0.5 V, the amounts of utilized zinc were 0.054 g and 0.072 g and the cut off voltage was reached within 6.5 and 9 min of discharge time for 98 % and 99.9 % pure zinc bromide salt solution respectively as shown in Fig. 2 a and b. The Faradic efficiency for the 99.9 % pure zinc bromide salt solution was approximately 1.4 times higher than that for 98 % pure zinc bromide salt solution. This is because of utilization of zinc from 99.9 % pure zinc bromide salt solution as calculated from the weight results, which was 10 wt % (49.96 wt %) higher than that for 98 % purity electrolyte (39.79 wt %).

As shown in Fig. 2 a and b, the slopes of the curves in the internal resistance (IR) region for both the electrolytes is same, 0.023, whereas in the diffusion limiting region of the 98 % purity electrolyte the slope is 0.66 times greater than that of the 99.9 % purity electrolyte. From the above observations, it is concluded that the internal resistance is not affected by impurities present in the electrolyte but the zinc deposition-dissolution processes are affected.

We must admit that no precise conclusion can be drawn from the above discussion until more specific experimental characterization has been carried out; hence EIS studies were performed. Accordingly the electrodes were charged galvanostatically at 20 mA to make 20 % of the theoretical capacity of the zinc active material. The impedance measurements were made at the same discharge current. The impedance data as shown in Fig. 3 reveal that the middle frequency semi-circle is related to charge transfer and the electrochemical double layer,

RSC Advances Accepted Manuscript

representing the kinetics of the zinc dissolution reaction and a typical Warburg semi infinite linear diffusion characteristic at low frequency part.

In the case of pure electrolyte the values of charge transfer resistance decrease due to the increase in the amount of zinc metal, while the value of capacitance increases. On the other hand in the case of impure electrolyte the value of charge transfer resistance increases due to decrease in the amount of zinc metal, while the value of double layer capacitance decreases. Fig. 3(i) shows electrode material (composite/graphite) independent high frequency response with 98 % pure electrolyte indicates that grains are less sensitive to fast switch of applied alternate electric field[7] due to impurity effect. On the other hand Fig. 3(ii) exhibits electrode material dependent high frequency response with 99.9 % pure electrolyte is due to less grain boundary contribution. For both composite and non porous graphite electrodes in 98 % pure electrolyte the low frequency spur as shown in Fig. 3(i) becomes larger indicating an increased grain boundary effect caused by more aggregation.[8]

The cycle test of the test cell with plastic carbon composite electrode and two different purity electrolytes was performed to investigate the variation of Faradaic efficiency versus cycle number as shown in Fig. 4. As the number of cycle increases, the discharge time also increases as seen in Fig. 4(i). The difference in Faradic efficiency between first and the sixth cycle for 99.9 % pure electrolyte is ~10 % whereas for 98 % pure electrolyte it is ~16 % (Figure 4(ii)). This can be ascertained due to the better utilization of Zinc in absence of impurities during charge discharge cycle. In general the deposition dissolution process is hindered by the impurities present in the 98 % pure electrolyte, hence the generated ions are smaller in number during dissolution process. Whereas in pure electrolyte, more ions are generated due to absence of impurity hindrance leading to fast dissolution; which is confirmed by lower R_{ct} values.

RSC Advances Accepted Manuscript

Fig. 5 a and b show the X-ray diffraction patterns of the zinc electrodeposits obtained from cells with 99.9 % and 98 % pure zinc bromide salt solution respectively. The sharpness of the diffraction peaks indicates zinc crystallization and it exhibits hexagonal structure. The observed, 'd' value is in good agreement with the standard values for zinc deposition (ASTM File No.1:*40831Zn). No impurity peak was observed. It exhibited that the reflection from (101) plane was more predominant compared to other peaks with an intensity ratio (I_{002}/I_{101}) 0.33:1, which approximates to the ratio of randomly oriented powder particles,[9] which is almost same for both the electrolyte. We choose the 101 line to calculate the grain size as it is prominent in all the patterns. The average crystallite size of the zinc deposit estimated from FWHM of (101) plane using Scherrer's formula is 124 and 103 nm for 98 % and 99.9 % pure zinc bromide salt solutions respectively. Fig. 6 shows the variation in ATC of the planes (002), (100), (101), (102), (103), (110) and (004) for Zn deposit obtained from both the zinc bromide salt solutions. The higher ATC values of the planes in pure zinc bromide salt solution with prominent for (004) plane is indicative of better deposition and higher crystalline nature of the zinc deposit grown. Fig. 7 a & b show the surface morphology of the zinc deposits obtained from both the electrolyte solutions. It is evident that the surface morphology of zinc deposit from the 98 % pure (Fig. 7 b) zinc bromide salt solution contains leaf like structure predominantly. Even though the difference in morphology is evident, it is difficult to exactly reason out for the gain in the faradic efficiency other than that of the role of impurity in deposition-dissolution process of zinc.[10]

The observed impurity through EDAX analysis (insert figure) is aluminum, copper and iron. The wt % of these impurities in 98 % purity electrolyte is 0.64, 1.11 and 0.39 respectively and in 99.9 % purity electrolyte 0.00, 0.89 and 0.26 respectively. Presence of aluminum in 98 % purity electrolyte appears to hinder zinc deposition-dissolution process.[11] The effect of impurity

RSC Advances Accepted Manuscript

is thus seen to be important when using carbon-plastic composite plates as electrode and future study will investigate the effect of other impurities using cyclic voltammetry studies. Absence of XRD peaks due to Al and other impurities infer that the impurities might be segregated in the non-crystalline region in grain boundary.[12]

Fig. 8 shows a typical cyclic voltammogram, at the scan rate of 5 mVs^{-1} , corresponding to zinc deposition on carbon composite electrode from a solution containing 2 M zinc bromide in 3 M NaCl as supporting electrolyte and 0.8 M N-ethyl N-methyl pyrolidinium bromide as complexing agent. No peak is observed during the cathodic scan but two crossovers at -1.091 V and at -1.025 V are observed owing to the formation of a new phase involving a nucleation process and equilibrium potential of Zn^{2+}/Zn redox couple respectively,[13] along with an anodic peak at -0.819 V. The observed crossover peak values fits well with the observed results on glassy carbon electrode[14] while anodic peak shifted by 100 mV towards positive side. The non appearance of the cathodic peak is due to the effect of pH as described elsewhere.[15]

When non porous graphite electrodes are used in the cell with 98 % pure zinc bromide salt solution, the cell exhibited twice the faradic efficiency of when compared with cell using carbon-plastic composite electrode and 99.9 % pure zinc bromide salt solution as shown in Fig. 2 c. The amount of reacted zinc is 0.111 g in 11 min which is almost equal to the theoretically calculated value of 0.112 g for the same time period which is 99.9 wt % of zinc utilization. From the slopes of the curves in IR (0.013) and diffusion controlled region (0.51239) as shown in Fig. 2 c, it can be ascertained that electrode material has an effect on the IR region (lower slope than carbon plastic composite electrode) than in the diffusion controlled region (same slope). From the above observations one can conclude that difference in internal resistance and Faradic efficiency is due to difference in resistivity of the electrode materials and active surface area

RSC Advances Accepted Manuscript

difference between the non porous graphite and carbon-plastic composite electrode materials[16] respectively.

Fig. 9 shows X-ray diffraction patterns of the zinc electrodeposits obtained from a cell with non porous graphite electrodes and 98 % pure zinc bromide salt solution. All peaks are accounted for zinc metal as that observed for carbon-plastic composite electrode. The predominant plane is again (101) and the average crystalline size of the zinc deposit estimated from FWHM is 103 nm as it was observed for carbon-plastic composite electrode with 99.9 % purity electrolyte. Even though the observed intensity of the basal and pyramidal planes is suppressed, the intensity ratio (I_{002}/I_{101}) 0.32:1 which is almost same as that obtained for carbon plastic composite electrodes. The order of reduction in ATC values of the planes to that of the composite electrode is (002), (101), (100) (102), (103), (110) and (004) as shown in Fig. 10. The preferential growth is along the (004) plane. The surface morphology is as shown in Fig. 11 a and b. Zinc deposit on non porous graphite produced a more compact deposit with a flake and leaf like structure. Thus, the change of substrate did not change the morphology but affected its compactness. Effect of impurity predominates when electronic conductivity and active surface of the substrate are low as that of carbon composite electrode, whereas this is not appreciable when substrate electronic conductivity and active surface are as high as that of non porous graphite electrode. Apart from this fact, compactness of the deposit also has a say by improving total conductivity than the loose structure.

The ATC values of zinc crystallographic planes on non porous graphite substrate after charge and discharge process are shown in Fig. 12. The difference in ATC values of the zinc deposit after charge and discharge processes are in the order (101), (002), (102), (100), (103), (004) and (110), whereas the order of difference in ATC values over carbon composite electrode

RSC Advances Accepted Manuscript

are (103), (002), (101), (102), (100), (110) and (004). On both the substrate materials the preferential orientation of the crystallites after discharge is (004). This observation is due to the presence of graphite materials as a filler to form a continuous conductive network through the composite plate.[17] Similarly, on both the substrate materials the basal plane (002) took second place in the order, which indicates that the preferential orientation of the covered surface is (004) basal plane parallel to the substrate surface with highest binding energy; hence, the total energy involved in the breaking of bonds for dissolution is higher and because of that electrochemically less reactive.[18] Conversely, with reference to (002) plane, there must be some crystallites present in the deposited zinc surfaces that are oriented at some angles apart from that parallel to the substrate plane resulting in electrochemical reaction.

Conclusion

An effect of zinc utilization and its performance characteristic have been reported. It was observed that simultaneously changing the quality of the electrolyte and electrode substrate material resulted in increase of the surface coverage with randomly oriented crystallographic (101) plane and as a result, exhibiting higher faradic efficiency. The enhanced ATC values of the planes in pure zinc bromide salt solution with prominent for (004) plane are evident for the better deposition and higher crystalline nature of the elemental zinc. Furthermore, EIS study infers that 98 % pure electrolyte favors grain boundary effect than 99.9 % pure electrolyte. Changing the substrate material to graphite plate increases the faradic efficiency even without changing the quality of the electrolyte resulting in 99.9 wt % of zinc utilization.

RSC Advances Accepted Manuscript

Acknowledgment

Authors Arulraj, Dheenadayalan and Ragupathy thank CSIR-TAPSUN project (NWP 56) for providing financial support. Dr. Vijayamohanan K. Pillai is acknowledged for his constant encouragement and support.

RSC Advances Accepted Manuscript

References

1. S. Kauff and K. Bolwin, *J. Power Sources,* 1992, **38**, 303-315.

2. H. Chena, T. N. Conga, W. Yanga, C. Tanb, Y. Lia and Y. Dinga, *Prog. Nat. Sci.*, 2009, **19**, 291-312.

3. K. T. Cho, P. Ridgway, A. Z. Weber, S. Haussener, V. Battaglia and V. Srinivasan, *J. Electrochem. Soc.,* 2011, **159**, A1806-A1815.

4. E. Lancry, B. Z. Magnes, I. Ben-David and M. Freiberg, *ECS Trans.*, 2013, **53,** 107-115.

5. R. Ramanauskas, P. Quintana, L. Maldonado, R. Pomés and M. A. Pech-Canul, *Surf. Coat. Technol.,* 1997, **92,** 16-21.

6. S. Ravindra Vaman, "*Investigation of transport processes and electrode kinetics in a zinc bromine battery*" (1991). Doctoral Dissertations, University of Connecticut, Paper AAI9215396.

7. D. He, M. Bligh and T. David Waite, *Environ. Sci. Technol.,* 2013, **47**, 9148-9156.

8. N. Hirose and A. R. West, *J. Am. Ceramic. Soc.,* 1996, **79**, 1633-1641.

9. L. M. A. Monzon, L. Klodt and J. M. D. Coey, *J. Phys. Chem. C.*, 2012, **116,** 18308-18317.

10. H. Nakano, S. Oue, K. Yanai, H. Fukushima, K. Nishina and N. Sogabe, *Journal of MMIJ*, 2011, **127,** 267-271.

11. F. W. Harris, 57th *General Meeting of the American Electrochemical Society*, St. Louis, Mo.,1930.

12. J. H. Lee and B. O. Park, *Thin Solid Films*, 2003, **426,** 94-98.

13. R. Greef, R. Peat, L. Peter and D. Pletcher, J. Robinson, *Instrumental Methods in Electrochemistry,* Ellis Horwood, Chichester, 1985, **Ch.9,** 283-316.

RSC Advances Accepted Manuscript

14. L. H. Mendoza-Huízar, C. H. Rios-Reyes and M. G. Gómez-Villegas, *J. Mex. Chem. Soc.*, 2009, **53**, 243-247.

15. L. Zhang, Q. Lai, J. Zhang and H. Zhang, *ChemSusChem*, 2012, **5**, 867-869.

16. B. C. H. Steele and A. Heinzel, *Nature,* 2001, **414**, 345-352.

17. R. Yeetsorn, M. W. Fowler and C. Tzoganakis, *Nanocomposites with Unique Properties and Applications in Medicine and Industry*, Edited by Dr. John Cuppoletti, 2011, **Ch.16**, 317-344.

18. J. C. Scully, *The Fundamentals of Corrosion*. 2nd edn., Oxford: Pergamon Press; 1990, 1-226.

RSC Advances Accepted Manuscript

Figure caption

1. Single cell assembly setup.
2. Discharge curves at a constant current density of 10 mA cm^{-2}; cell with carbon-plastic composite electrodes and 98 % purity zinc bromide electrolyte (a), cell with carbon-plastic composite electrodes and 99.9 % purity zinc bromide electrolyte (b) cell with non porous graphite plate electrodes and 98 % purity zinc bromide electrolyte (c).
3. Nyquist plot of $ZnBr_2$ flow cell containing 98 % (a) and 99.9 % (b) pure $ZnBr_2$ in graphite and composite electrodes.
4. Charge discharge curves of $ZnBr_2$ flow cell containing 99.9 % pure $ZnBr_2$ as electrolyte (a) and Faradic efficiency as function of cycle number for both 98 % and 99.9 % pure $ZnBr_2$ (b).
5. XRD patterns for Zn deposit obtained from the cell made with carbon-plastic composite electrodes and 98 % purity zinc bromide electrolyte (a) and 99.9 % purity zinc bromide electrolyte (b).
6. Absolute texture coefficient values of the Zn crystallographic planes for deposit obtained from cell with carbon-plastic composite electrodes from 98 % and 99.9 % purity zinc bromide electrolyte.
7. SEM images of the zinc deposit from cell with carbon-plastic composite electrodes and 98 % purity zinc bromide electrolyte (a) and from cell with carbon-plastic composite electrodes and 99.9 % purity zinc bromide electrolyte (b).
8. Cyclic voltammogram obtained from carbon-plastic composite electrode 2 M zinc bromide in 3 M NaCl as supporting electrolyte and 0.8 M N-ethyl N-methyl pyrolidinium bromide as a complexing agent and at a potential scan rate of 5 mV s^{-1}.

RSC Advances Accepted Manuscript

9. XRD pattern obtained for Zn deposit obtained from cell with non porous graphite electrodes and 98 % pure zinc bromide electrolyte.
10. Absolute texture coefficient values of the Zn crystallographic planes for deposit obtained from cell with non porous electrodes and 98 % pure zinc bromide electrolyte.
11. SEM pictures of Zn deposit obtained from cell with non porous electrodes and 98 % purity zinc bromide electrolyte (a) and Zn deposit obtained from cell with composite carbon electrodes and 98 % purity zinc bromide electrolyte (b).
12. Absolute texture coefficient values of the zinc crystallographic planes for deposit obtained from cells carbon composite electrode (a) and non porous graphite electrode (b) with 98 % pure electrolyte solution after charge- discharge process.

RSC Advances Accepted Manuscript

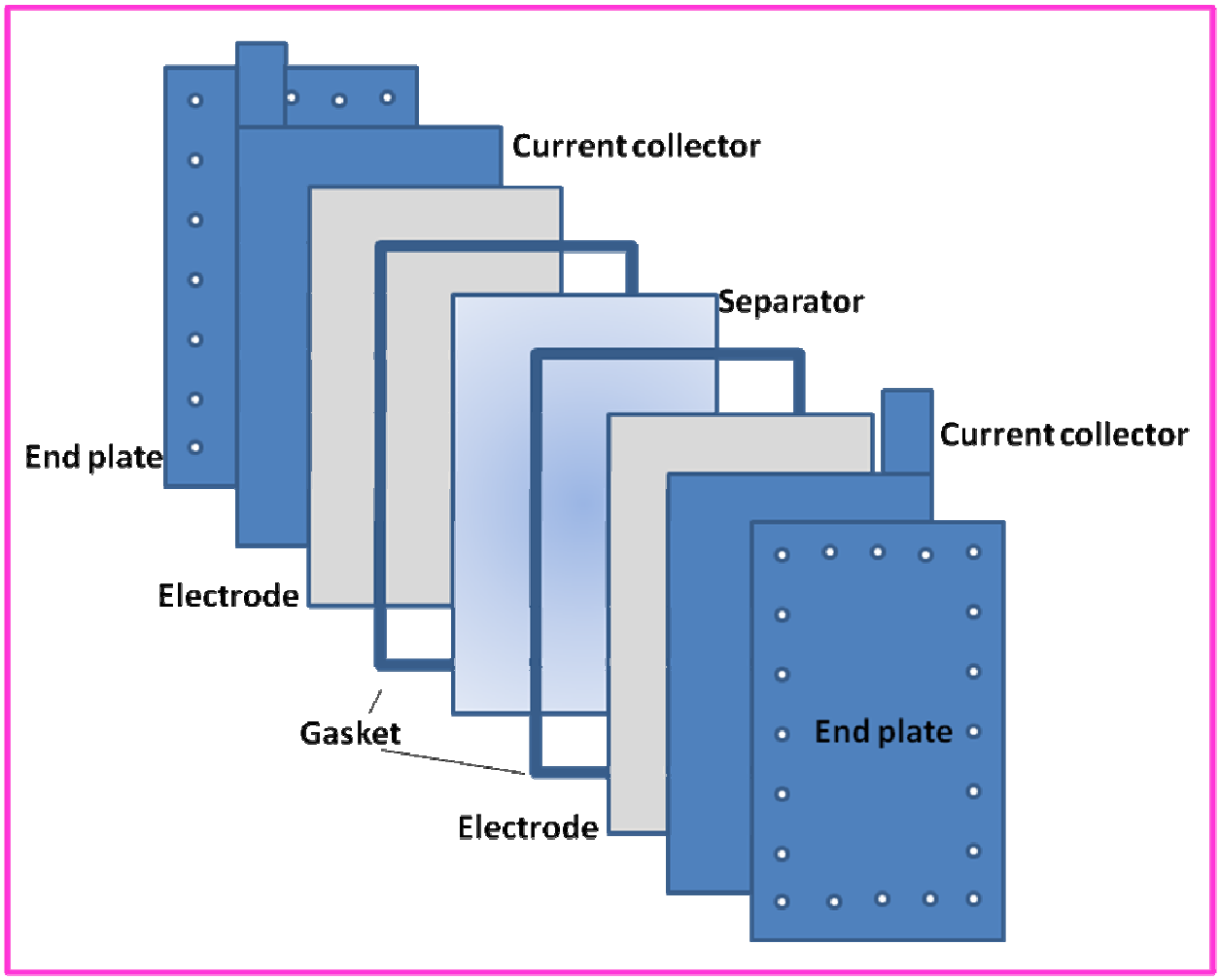

Figure 1

RSC Advances Accepted Manuscript

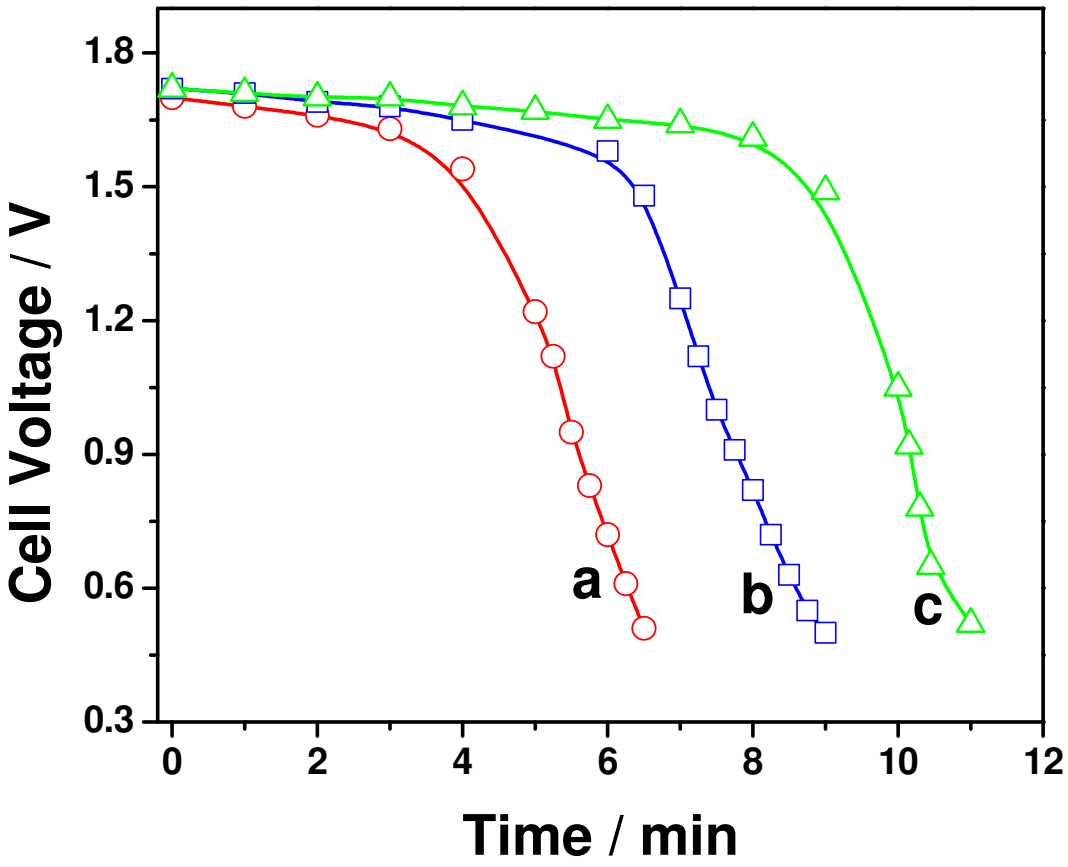

Figure 2

RSC Advances Accepted Manuscript

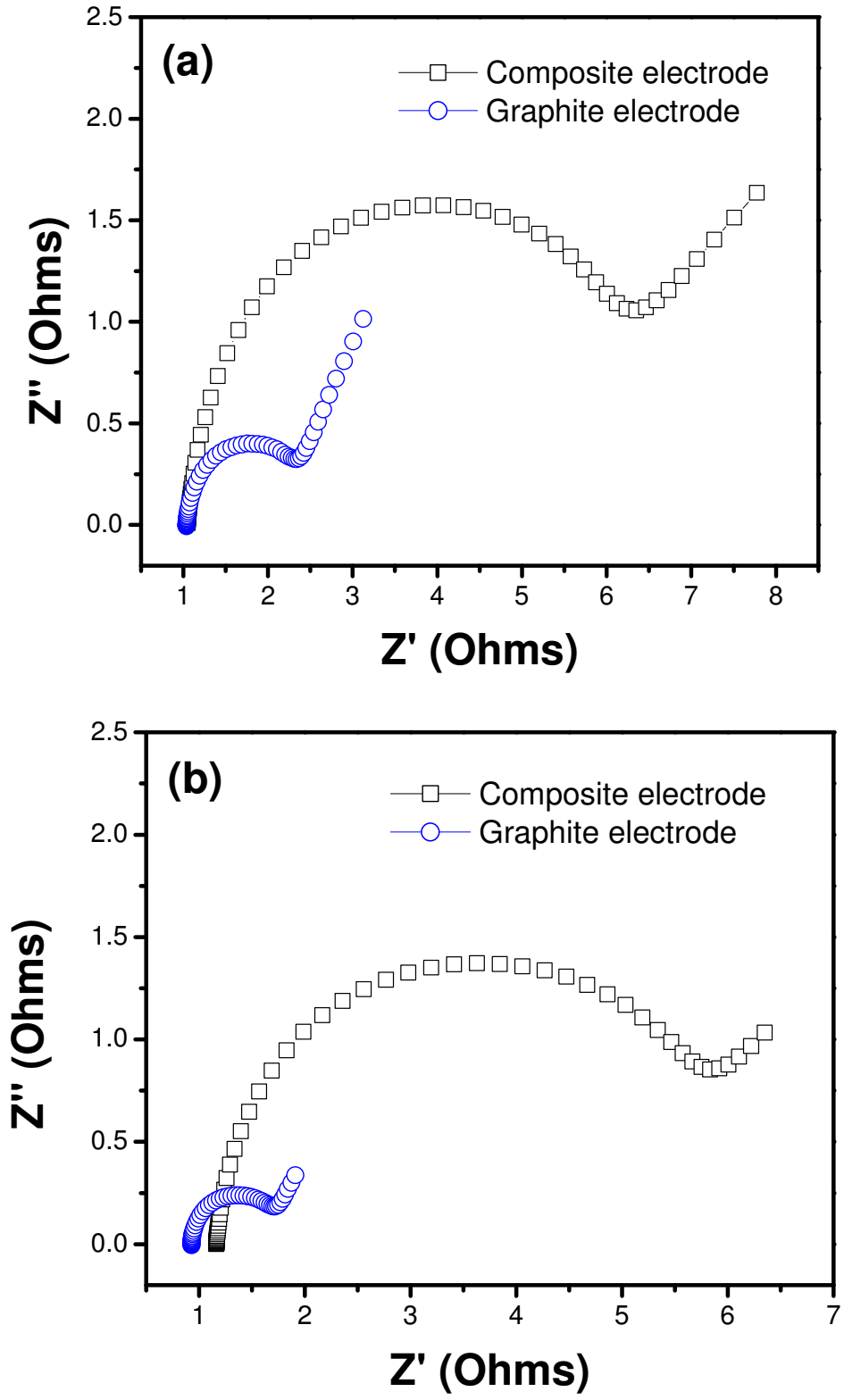

Figure 3

RSC Advances Accepted Manuscript

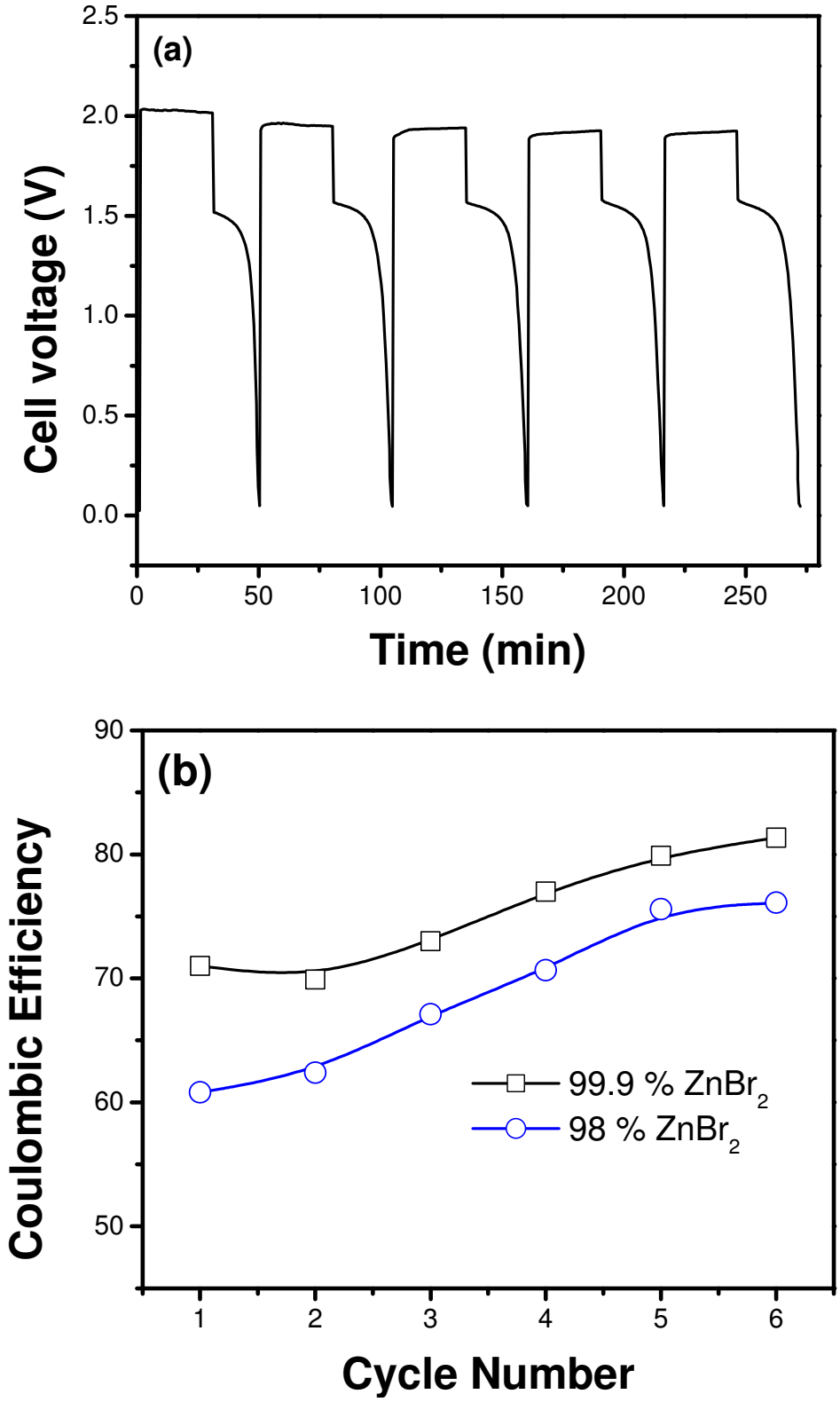

Figure 4

RSC Advances Accepted Manuscript

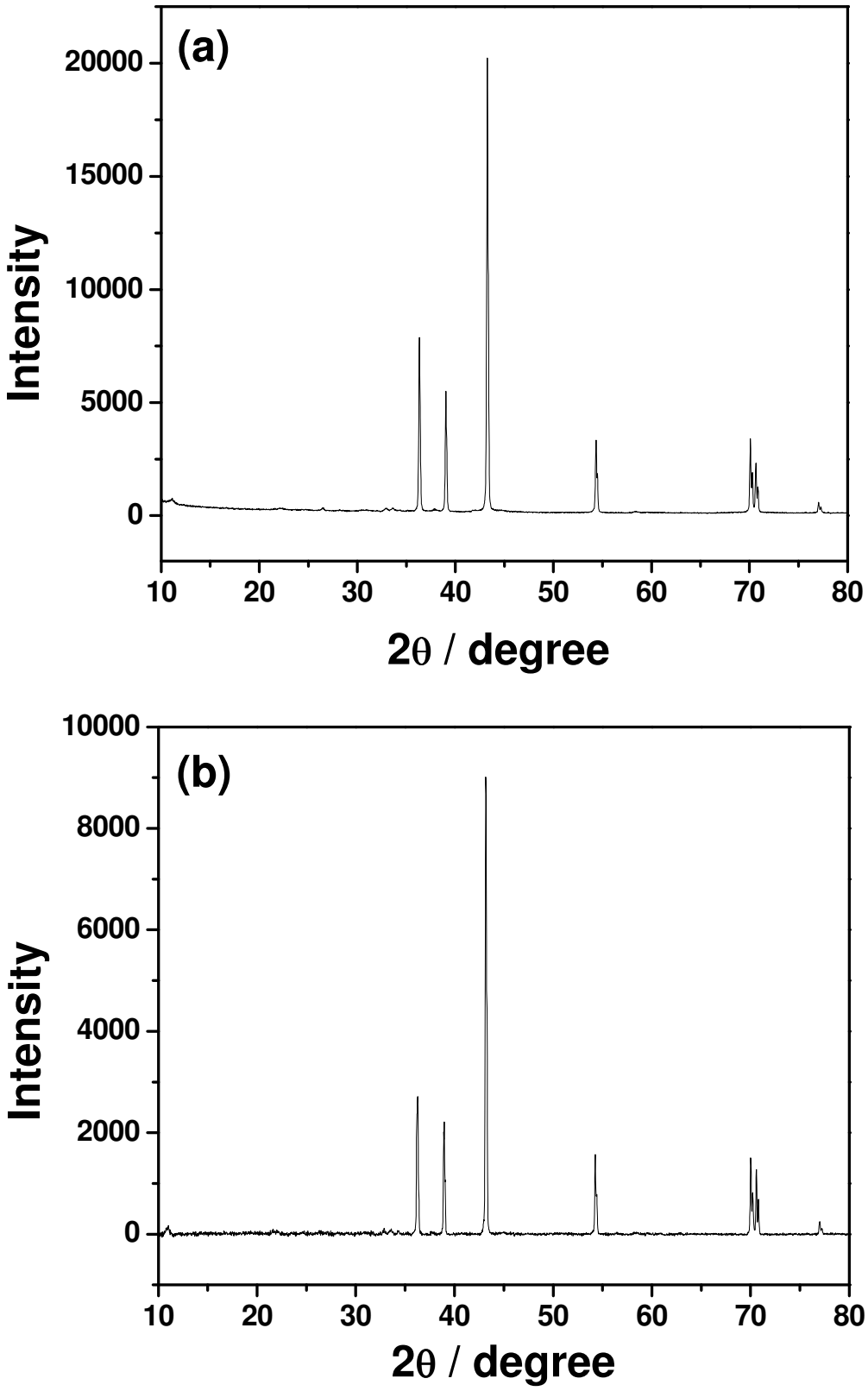

Figure 5

RSC Advances Accepted Manuscript

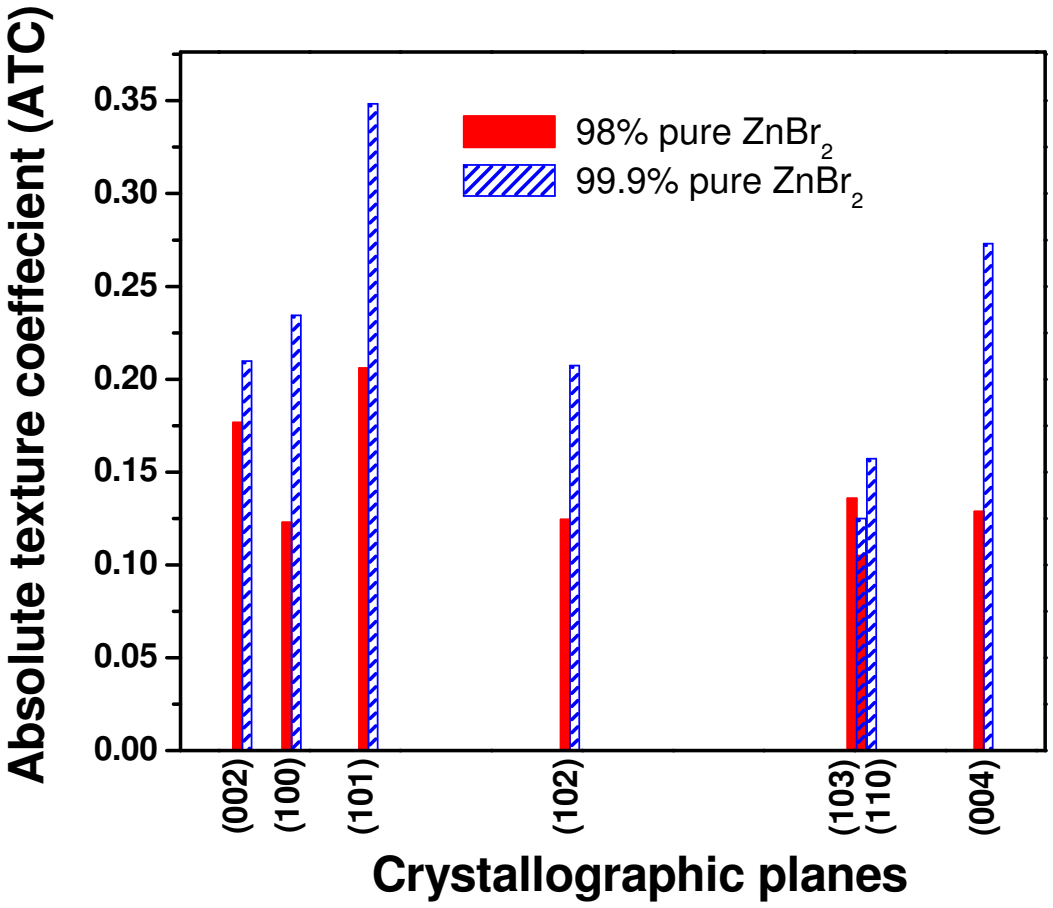

Figure 6

RSC Advances Accepted Manuscript

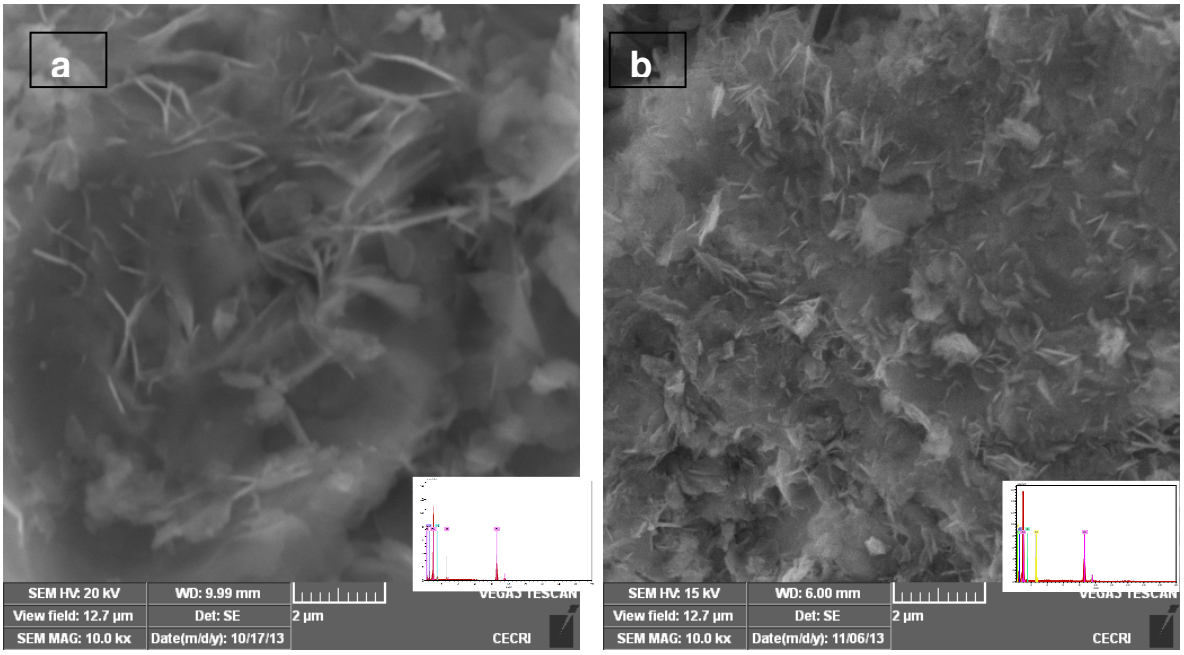

Figure 7

RSC Advances Accepted Manuscript

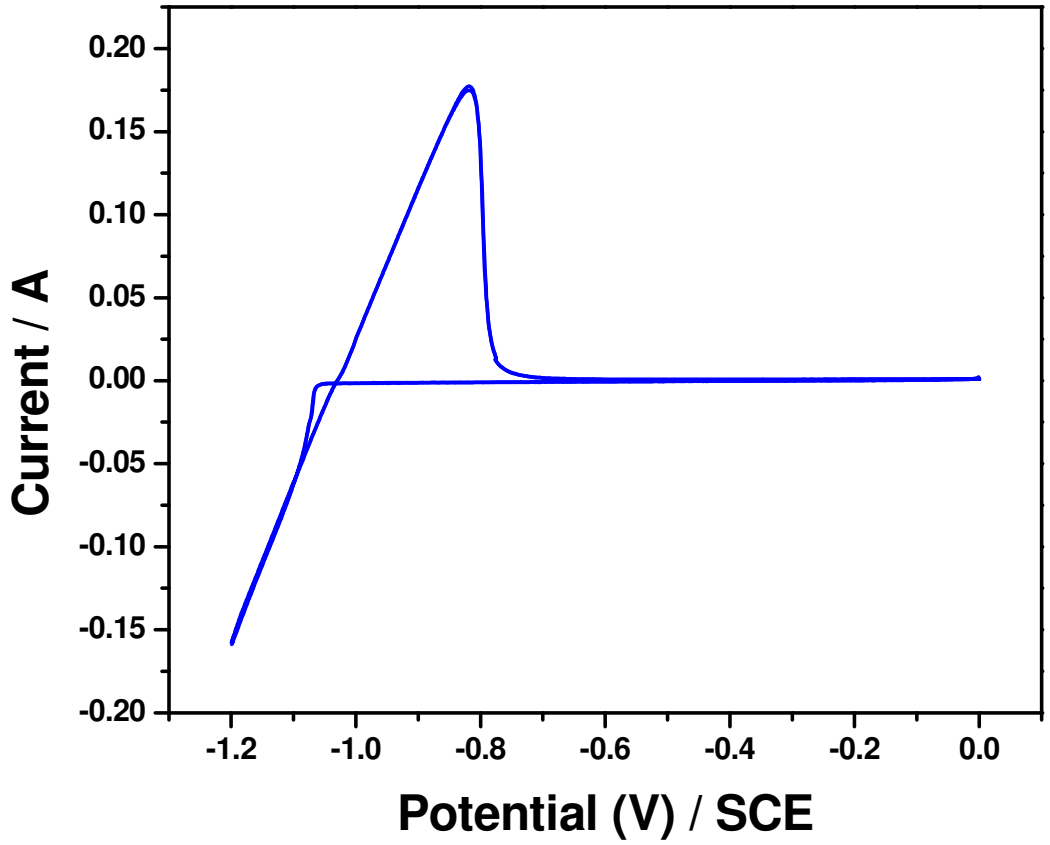

Figure 8

RSC Advances Accepted Manuscript

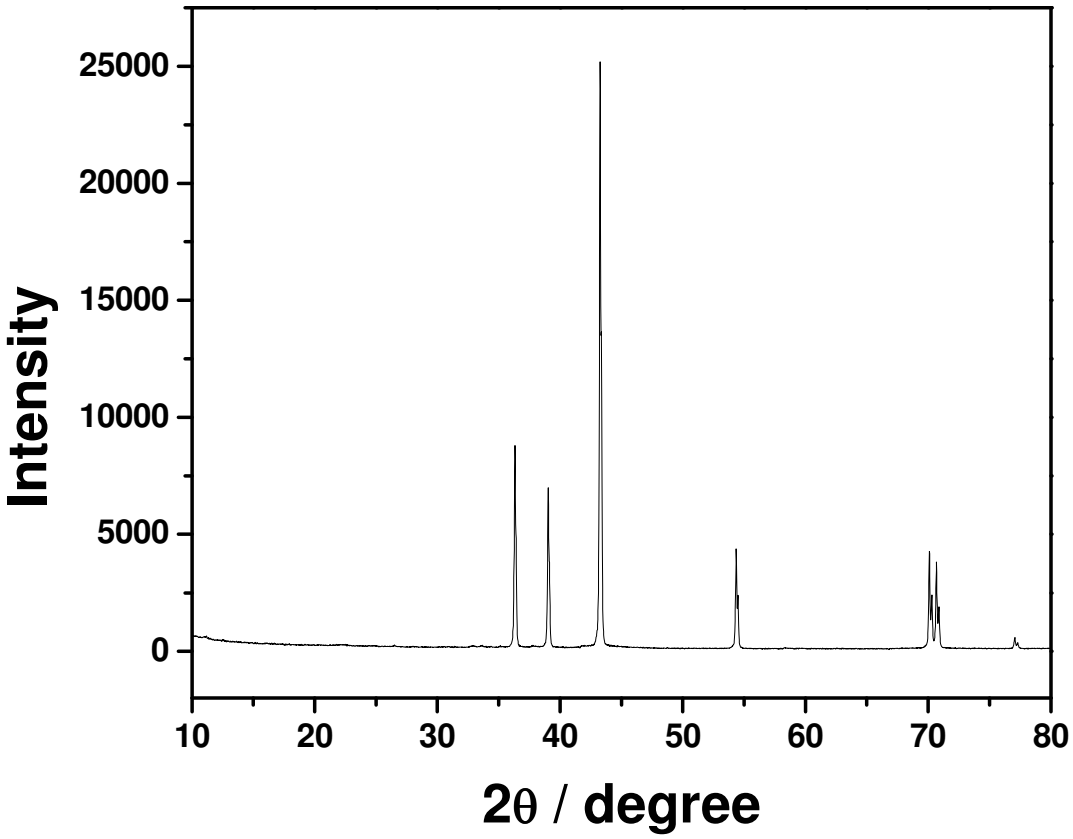

Figure 9

RSC Advances Accepted Manuscript

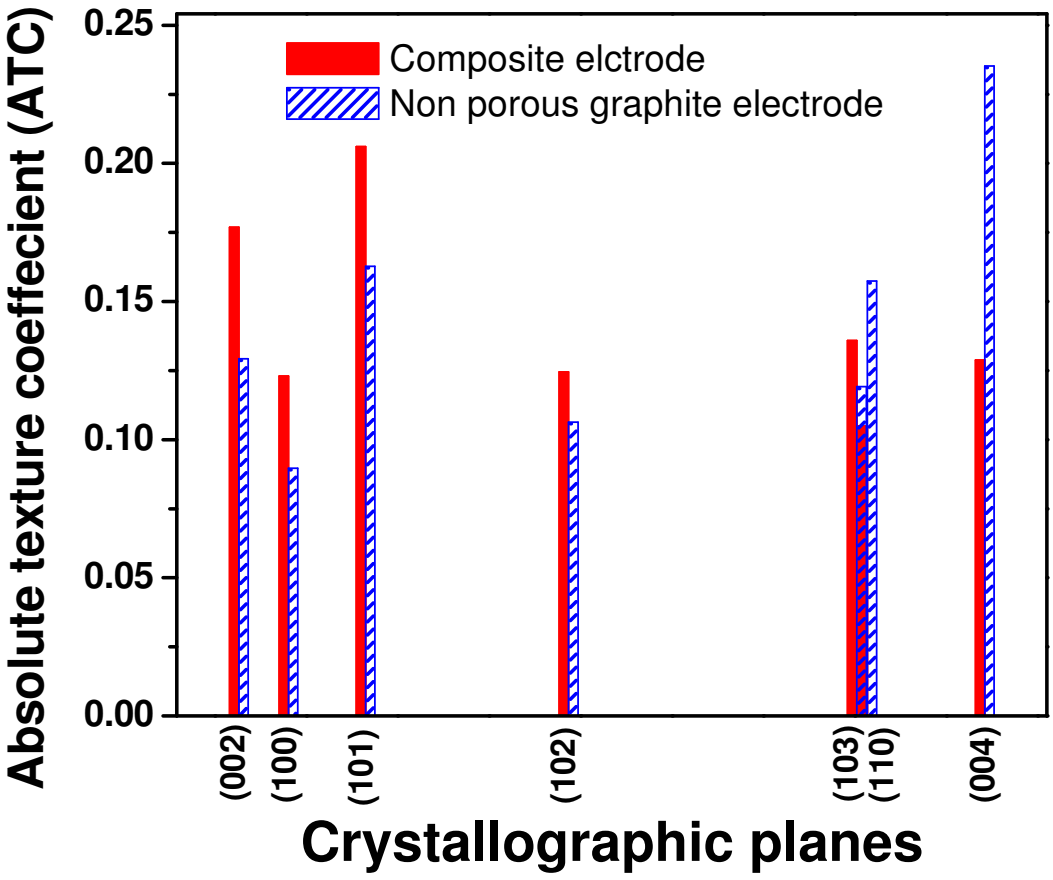

Figure 10

RSC Advances Accepted Manuscript

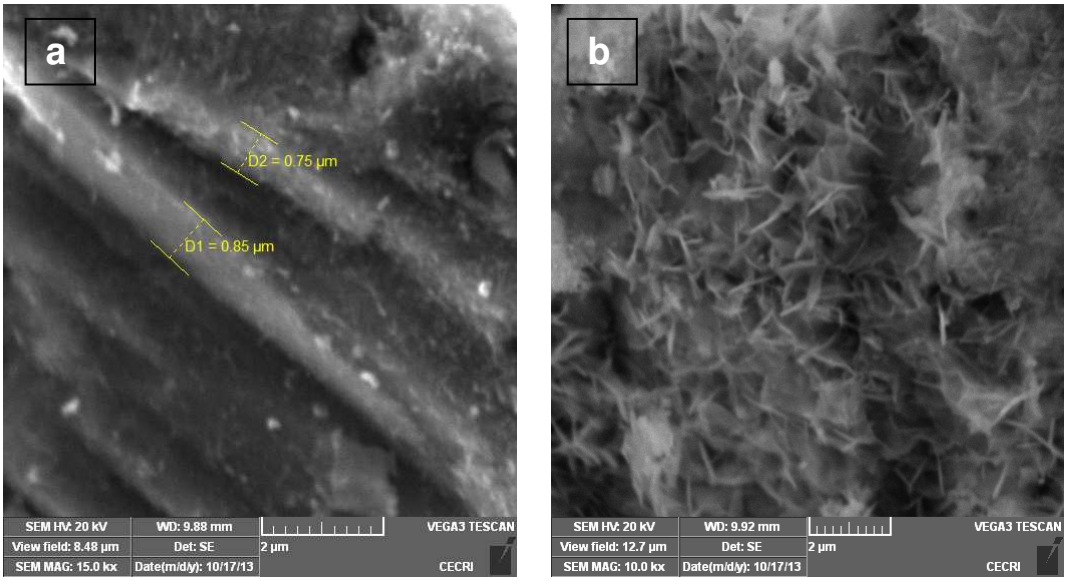

Figure 11

RSC Advances Accepted Manuscript

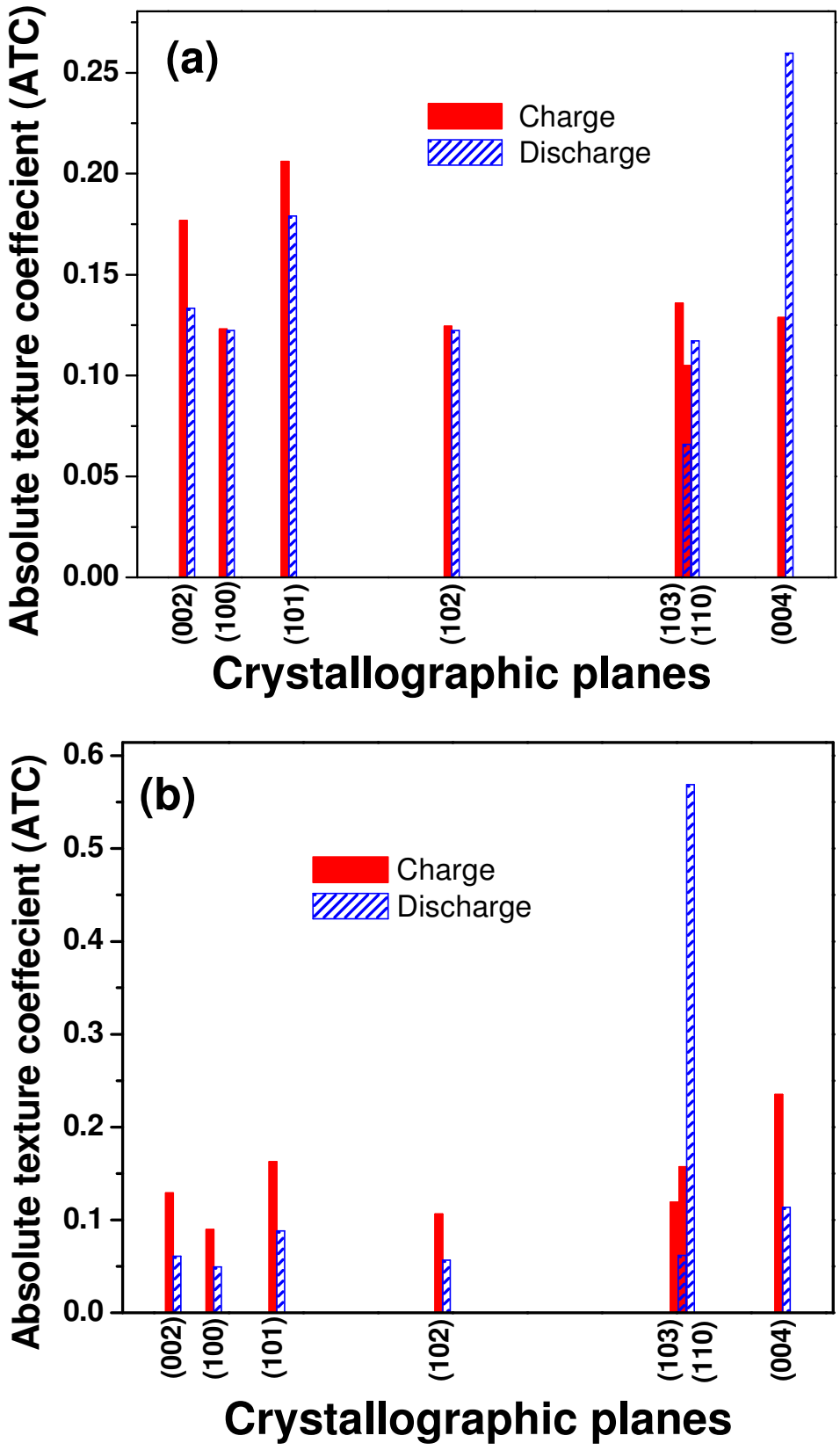

Figure 12

RSC Advances Accepted Manuscript